DOI 10.5162/iCCC2024/7.2

Integration concept of plasmonic TiN nanohole arrays in a 200 mm BiCMOS Si technology for refractive index sensor applications

J. Jose[(1)]; C. Mai[(1)]; S. Reiter[(2)] ; C. Wenger[(1, 2)]; I. A. Fischer[(2)]

(1) IHP - Leibniz-Institut für innovative Mikroelektronik, 15236 Frankfurt (Oder), Germany
(2) BTU Cottbus-Senftenberg, 03046 Cottbus, Germany

Abstract

In this work, we present an integration concept for plasmonic Titanium Nitride (TiN) nanohole arrays (NHA) into a 200 mm BiCMOS silicon (Si) technology. For the fabrication of a TiN NHA, we investigated the TiN layer surface roughness in dependence on different process variations. Moreover, we developed a process module to release the TiN NHA to enable a direct contact with materials to be analyzed. By using an amorphous silicon (a-Si) stop layer, we are able to realize a controlled stop at the bottom level of the TiN NHA.

1. Introduction

Over the past ten years, sensor devices have attracted a lot of attention since they are becoming essential instruments for a wide range of applications (1). Optical sensors based on plasmonic excitations have attracted much of interest, especially in the environmental and biomedical fields, because of their high sensitivity, high specificity, and quick detection times (2). Utilizing the optical phenomena generated either by propagating localized plasmons inside metallic nanostructures or by surface plasmon polaritons (SPP) at a metallic dielectric interface, these sensors are able to detect bulk or surface refractive indices (RI) changes (3).

Metallic nanohole arrays have emerged as interesting possibilities in this context. By the top illumination with incident light, NHAs exhibit extraordinary optical transmission (EOT), characterized by pronounced transmission peaks at specific wavelengths determined by the NHA's geometry parameters (4). These peaks will be shifted by a change in the refractive index of the adjacent dielectric material.

Integration of an NHA above a photodetector facilitates the direct conversion of an optical signal to an electrical current, offering the promise of compact and cost-effective refractive index sensors. However, the integration of these components within CMOS-compatible 200 mm wafer silicon technology presents significant challenges.

Numerous studies have investigated the integration of germanium (Ge) photodetectors with metallic NHAs to develop plasmonic refractive index sensors (5–8). Ge photodetectors were realized by a mesa structure whose layer stack was deposited by molecular beam epitaxy (MBE). The NHAs are patterned within aluminum (Al) layers deposited via metal evaporation, serving both as the NHA material and for metallization. However, this approach is incompatible to 200 mm wafer BiCMOS silicon technologies. The deposition of the photodetector stack by MBE is a very expensive process and uncommon for an industrial fabrication. Moreover, the metallization of these technologies occurs during the Back End of Line (BEOL) process which comprises the production of multiple metal layers separated by interlayer dielectric (ILD) stacks.

To realize an RI sensor by combining NHAs with photodetectors, it's essential to fabricate both components with a low vertical distance to each other. Additionally, it is essential to enable the NHA in direct contact with the materials to be analyzed. However, the Ge photodetector is produced during the Front End of Line (FEOL) process. In respect to a CMOS compatible 200 mm Si technology, the NHAs positioned close to the photodetector will be encapsulated by ILD stacks needed for the BEOL. Hence, it is necessary to release the NHA by removing the ILD stack, which is essential for their proper functioning. Figure 1 illustrates the integration concept of the RI sensor.

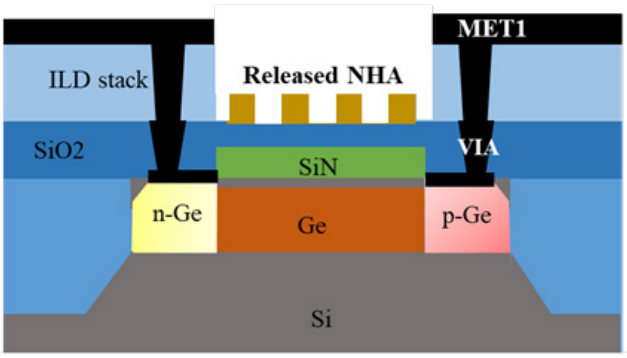

Figure 1: Illustration of the integration concept for an RI sensor in CMOS compatible 200 mm Si technology

This paper presents investigations concerning the process integration of Titanium Nitride nanohole arrays into a 200 mm BiCMOS Si technology. TiN stands out as a highly promising metallic alloy due to its exceptional thickness uniformity and minimal surface roughness (9). Previous research has demonstrated the advantageous plasmonic properties of TiN NHAs (10).

In this work, we investigate the structural properties of TiN NHAs in dependence to different process variations. Furthermore, we developed a release module which allows a controlled stop at the bottom level of the TiN NHA. This

process concept is the next step for the integration of RI sensors in a 200 mm BiCMOS Si technology.

2. Process description

2.1. TiN NHA fabrication

A concept for the NHA fabrication was already presented in Reference 9. In this work we tried to reproduce these results, but additionally we investigate further process variations. We utilized a 760 µm thick silicon wafer substrate for our experiments. Figure 1 illustrates a schematic overview of the sequential processes involved. The first process step comprised a deposition of a 200 nm thick silicon dioxide (SiO_2) layer. This procedure was carried out either by Plasma-Enhanced Chemical Vapor Deposition (PE CVD) or a Sub-Atmospheric Chemical Vapor Deposition (SA CVD), to check a potential impact on the growth behavior of the TiN.
Afterwards, a TiN layer was deposited via a sputtering process. Various sheet thicknesses of 40 nm, 80 nm and 150 nm were realized.
By applying a reactive ion etching (RIE) procedure, we structured the NHA in the TiN layer over a resist mask patterned before by a 248nm deep ultraviolet (DUV) lithography. All process variations are summarized in Table 1.

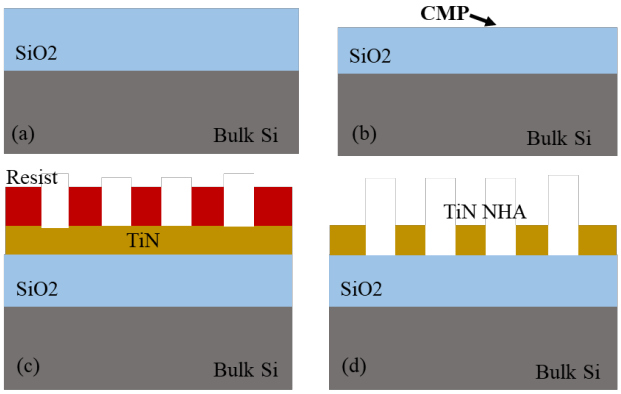

Figure 2: Process steps for the fabrication of TiN NHA (a) deposition of SiO2 (b) Chemical mechanical polishing (c) deposition of TiN layer and DUV lithography (d) pattering of TiN NHA by RIE

Oxide layer underneath	TiN layer thickness (nm)
PE-TEOS	40
PE-TEOS	80
PE-TEOS	150
SAUSG	40

Table 1: Process variants for TiN roughness analysis

2.2. TiN NHA Release

The development of the process module to release the TiN NHA is based on the implementation of a stop layer. After the NHA fabrication, we deposited a 30 nm thick amorphous silicon layer by PE CVD (Fig. 3a). By using a resist mask, the a-Si layer was thus structured by an RIE procedure to keep it locally above the NHA (Fig. 3b). Afterwards, we carried out a certain sequence of steps to emulate the process situation after finishing the metallization. We deposited a SiO_2 as the ILD stack. Subsequently, a Chemical Mechanical Polishing (CMP) step has been carried out to planarize the surface of oxide. Finally, a silicon nitride was deposited, which serves as the equivalent of the passivation layer for metallization. The NHA was then exposed via an RIE step using a resist mask. The RIE process was stopped by time at a residual oxide thickness above the NHA in the range of 100 nm to 150 nm (Fig 3c). A further chemical wet etching with hydrofluoric acid (HF) was carried out to remove the remaining oxide with a high selectivity to silicon nitride and silicon. For this process step, the a-Si sheet act as a stop layer. For the removal of the a-Si layer, an ACTUP935 clean was performed (Fig. 3d).

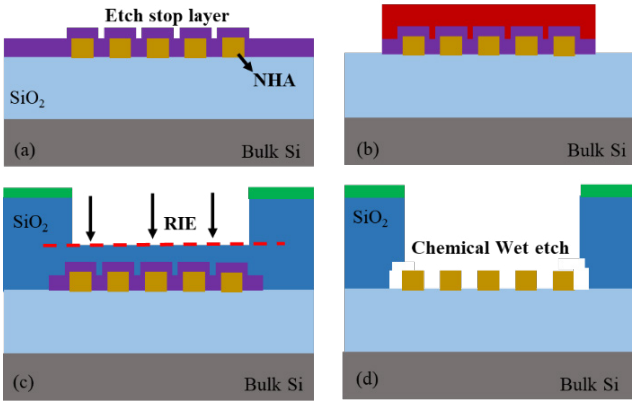

Figure 3: Illustration of Concept for exposing NHA using an a-Si stop layer a) Deposition of a-Si stop layer, b) Structuring of a-Si stop layer; c) Deposition of ILD stack and silicon nitride and following RIE of Oxide c) Wet chemical etching of a-Si

3. Results and discussion

3.1. NHA fabrication

For the structural analysis of the TiN NHAs, we measured the surface roughness of the TiN layer using atomic force microscopy (AFM) before the NHA structuring. As depicted in Table 2, the lowest roughness we received for the process variation with the thinnest TiN layer deposited on a PE CVD oxide. In comparison to the process flow using an SA CVD oxide as the material below the TiN layer, the roughness of TiN surface is much increased. We believe that the surface roughness of TiN layers formed on SA CVD and PE CVD oxide can be linked to a number of factors, including the sheet quality of the passivation oxide layers. Research has been conducted to evaluate the deposition characteristics of TEOS oxide films fabricated through PE CVD and SA CVD methodologies. Plasma deposition is observed to enhance both gas-phase and surface reactions, yielding films of better sheet quality. Notably, TEOS films deposited via plasma exhibited

superior sheet quality (11). To determine the particular mechanism underlying the observed variation in TiN surface roughness, more research into the interactions between the oxide layer underneath and the TiN deposition process is required.
In dependence to the TiN thickness, the surface roughness exhibited an increasing root mean square for thicker TiN layers. Same behavior occurred in previous publication (12). It must be noted, our TiN layers are really smooth, even smoother than what others have done before (13, 14). In a previous investigation (reference 10), we fabricated sputtered TiN films with thicknesses of 50 nm, 100 nm, and 150 nm. It was observed that the surface roughness of these TiN layers increased proportionally with thickness. Despite this trend, all fabricated films displayed a low surface roughness, with the highest measured root mean square (RMS) value being 1.277 nm. This indicates a relatively smooth surface for all TiN films produced. We successfully replicated these findings in our investigation.

Oxide layer underneath	TiN layer thickness (nm)	Surface roughness, RMS (nm)
PE-TEOS	40	0.739
PE-TEOS	80	1.001
PE-TEOS	150	1.415
SAUSG	40	2.331

Table 2: Process variants for TiN roughness analysis

Figure 4 shows the cross-section of the structured NHA, which is captured by the transmission electron microscope (TEM). In regard to the structuring of the NHA we could reproduce the results presented in Ref. (9). We measured similar angles for the TiN sidewalls of around 5.5 degrees.

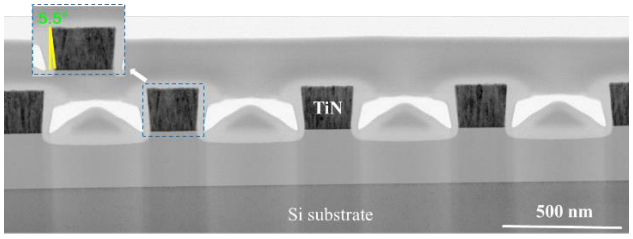

Figure 4: TEM image of the Cross section of the NHA structured in 150 nm thick TiN

3.2. NHA release

In our investigation of the release module, we first inspected the NHAs after the deposition of the 30 nm thick a-Si layer. We observed a good edge conformity, which implies a uniform deposition rate both vertically and laterally. We measured a 22 nm lateral and 27 nm vertical deposition thickness which implies, around 80 % edge conformity (Fig 5).
In a separate experiment, we performed a thorough assessment of the a-Si layer's robustness on a different wafer where it was deposited directly onto a TiN nanohole array without additional structuring. Subsequently, the sample underwent an extended 10-minute chemical wet HF etch to observe for potential adverse effects, such as cracks in the a-Si layer which could result in voids caused by wet etching of the oxide beneath the a-Si layer. Impressively, no such issues were found, confirming the robustness and reliability of the a-Si layer in our processes.

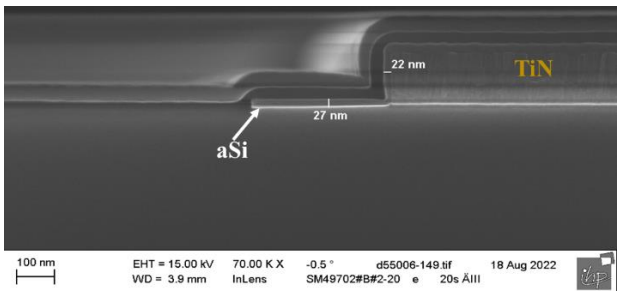

Figure 5: SEM image of structured a-Si layer over the TiN NHA after the deposition of a decoration layer stack.

The total ILD stack thickness to be removed was around 950 nm. This stack comprises 380 nm silicon nitride, 420 nm Silicon oxide and 150 nm Silicon oxide inside the nanoholes. Further RIE step was stopped by time and halted at around 180 nm of oxide above the a-Si layer. The residual 180 nm oxide was subsequently removed by a chemical wet etch with HF acid, for about 5 minutes.
Furthermore, upon removing the a-Si stop layer using ACTUP935 etch, we conducted AFM surface roughness measurements on the released TiN surface. Remarkably, the deposition and removal of a-Si had no visible impact on the roughness of the TiN surface. The RMS roughness remained consistent at 1.318 nm (Fig. 6) post a-Si deposition, compared to 1.415 nm prior, indicating a negligible deviation of less than 10 percent.
This release process was executed flawlessly, resulting in the complete removal of all dielectric layers above the NHA and facilitating the precise exposure of the NHA.

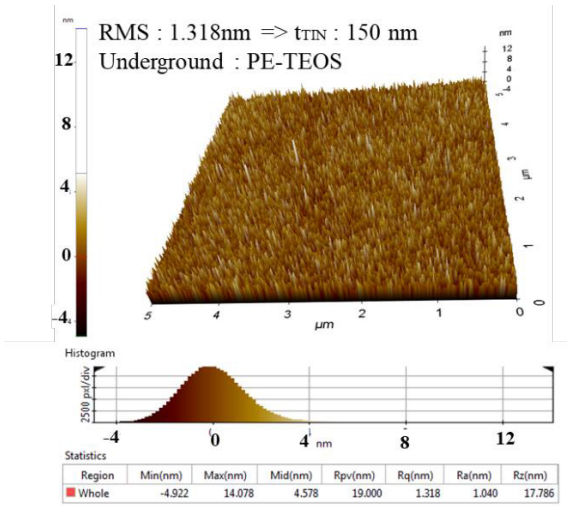

Figure 6: AFM measurement of TiN surface after release

Figure 7 shows the SEM cross section image of the released NHA and demonstrates the effectiveness of using a-Si as an etch stop layer providing better consistency and

accuracy during the NHA release process without any under etching of oxide below the NHA.

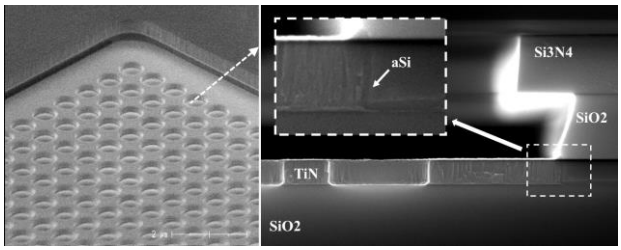

Figure 7: SEM image of Top view and Cross section of the TiN NHA after the release procedure

4. Conclusion

Our study presents a novel integration concept for plasmonic TiN nanohole arrays into a CMOS-compatible 200 mm wafer Si technology. We have developed a process module to release TiN NHA by the utilization of an amorphous silicon stop layer. Through careful inspection of the surface roughness by AFM, no impact on the structural characteristics of the TiN surface could be observed. Specifically, our results highlight the possibility of utilizing amorphous silicon as an etch stop layer, exhibiting efficient release of NHA. This effort is a major step toward the co-integration of TiN NHAs and Ge photodetectors for the fabrication of refractive index sensors in a 200 mm wafer BiCMOS Si technology.

5. Acknowledgement

This work has been funded by the Federal Ministry of Education and Research of Germany (BMBF) within the iCampus2 project, grant number 16ME0424.

6. Literature

[1] X. Wang, J. Zhu, X. Wen, X. Wu, Y. Wu, Y. Su, H. Tong, Y. Qi and H. Yang, Opt. Mater. Express, 9(7), 3079 (2019).

[2] X. Wang, J. Zhu, Y. Xu, Y. Qi, L. Zhang, H. Yang and Z. Yi, Chinese Phys. B, 30(2), 24207 (2021).

[3] Z. Chen, P. Li, S. Zhang, Y. Chen, P. Liu and H. Duan, Nanotechnology, 30(33), 335201 (2019).

[4] J. Yu, J. Zhu, S. Ye and X. Wang, Results in Physics, 26(1), 104396 (2021).

[5] L. Augel, R. Korner, S. Bechler, J. Schulze and I. A. Fischer, in GFP: 14th International Conference on Group IV Photonics : 23-25 August, Grand Hyatt Berlin, Germany, p. 161, IEEE, Piscataway, NJ (2017).

[6] L. Augel, S. Bechler, R. Korner, M. Oehme, J. Schulze and I. A. Fischer, in 2017 International Electron Devices Meeting: Technical digest, 40.5.1-40.5.4, IEEE, Piscataway, NJ (2017).

[7] F. Berkmann, L. Augel, M. Hack, Y. Kawaguchi, D. Weishaupt, I. A. Fischer and J. Schulze, IEEE Photonics J., 14(3), 1–8 (2022).

[8] L. Augel, Y. Kawaguchi, S. Bechler, R. Körner, J. Schulze, H. Uchida and I. A. Fischer, ACS Photonics, 5(11), 4586–4593 (2018).

[9] C. Mai, S. Marschmeyer, A. Peczek, A. Kroh, J. Jose, S. Reiter, I. A. Fischer, Ch. Wenger, A. Mai, ECS (2022).

[10] S. Reiter, W. Han, C. Mai, D. Spirito, J. Jose, M. Zöllner, O. Fursenko, M. A. Schubert, I. Stemmler, C. Wenger and I. A. Fischer, Plasmonics, 7(2), 152 (2023).

[11] S. Nguyen1, D. Dobuzinsky1, D. Harmon1, R. Gleason1 and S. Fridmann1, Journal of The Electrochemical Society, 137, DOI 10.1149/1.2086914 (1990).

[12] H. Liang, J. Xu, D. Zhou, X. Sun, S. Chu and Y. Bai, Ceramics International, 42(2), 2642–2647 (2016).

[13] Z.-Y. Yang, Y.-H. Chen, B.-H. Liao and K.-P. Chen, Opt. Mater. Express, 6(2), 540 (2016).

[14] C.-C. Chang, J. Nogan, Z.-P. Yang, W. J. M. Kort-Kamp, W. Ross, T. S. Luk, D. A. R. Dalvit, A. K. Azad and H.-T. Chen, Scientific reports, 9(1), 15287 (2019).